Title

Point-of-use printed nitrate sensor with desalination units

Journal

Microchimica Acta, 189(6)

ISSN

0026-3672

Authors

Wu, Shuo-En
Shiller, Alan
Barnard, Andrew
et al.

Publication Date

2022-06-01

DOI

10.1007/s00604-022-05314-5

Peer reviewed

Microchimica Acta (2022) 189:221
https://doi.org/10.1007/s00604-022-05314-5

ORIGINAL PAPER

Point-of-use printed nitrate sensor with desalination units

Shuo-En Wu[1] · Alan Shiller[2] · Andrew Barnard[3] · Jason D. Azoulay[4] · Tse Nga Ng[1,5]

Received: 29 November 2021 / Accepted: 19 April 2022

Abstract
Nitrate is an important marker of water quality that can be challenging to detect in seawater due to the presence of multiple chemical interferants and high background chloride. Here, we demonstrate a compact microfluidic device that incorporates electrochemical desalination to selectively remove the interfering chloride ions and improve the detection limit of the downstream potentiometric nitrate sensor. The microfluidic platform was fabricated by a low-cost cut-and-lamination approach, and the detection mechanism was based on potentiometric measurements at an Ag/AgCl electrode coated with a nitrate-selective membrane. The sensor system achieved a detection limit of 0.5 mM with a sensitivity of 11.3 mV/dec under continuous flow.

Keywords Nitrate · Desalination · Additive fabrication

Introduction

Monitoring dissolved nitrate levels in the environment is critical for understanding ecosystem issues such as eutrophication that can lead to fish kills and declines in oyster harvests [1–5]. In addition to environmental impacts, excessive nitrate in drinking water can lead to serious health problems including gastric cancer and infant methemoglobinemia [6]. Therefore, it is desirable to enable facile nitrate measurements for water quality monitoring at the point of use and in real-time. Traditional chromatography techniques [7, 8] used to determine nitrate levels are limited by time-consuming and bulky setups that restrict analysis to laboratory settings. In order to facilitate in situ real-time monitoring, electrochemical sensors based on ion-selective membranes (ISM) [2, 9] offer the advantages of reduced size, weight, and cost for the development of systems that can be more readily deployed. However, nitrate measurements based on ISMs are vulnerable to chemical interferants such as anions [10, 11] and have primarily been utilized in freshwater environments with low salt concentrations. As a result, low sensitivity and poor detection limits were observed in potentiometric ISM sensors when used to examine wastewater or seawater with high chloride concentrations.

A sample treatment process to remove chloride anions can be an effective approach to mitigate the problem of interference that results from high chloride concentrations and prevents the ISM sensor from detecting nitrate. However, typical desalination technologies such as reverse osmosis, electrodialysis, and distillation are non-selective in their ion removal and would concurrently decrease the concentration of nitrate. To selectively remove chloride, a desalination approach based on a microfluidic platform has been demonstrated by oxidizing chloride anions on silver electrodes resulting in AgCl solids [12–14]. This reversible electrochemical process is specific to the removal of chloride from solution without the loss of nitrate [13]. Prior microfluidic desalination prototypes involve machining of plexiglass or molding of polydimethylsiloxane [15]; however, this poses challenges for embedding electronic components [16–18]. Here, we present a microfluidic platform built with cutting and lamination [19–21] of poly(ethylene terephthalate) (PET) films, which are compatible with additive printing

✉ Tse Nga Ng
tnn046@ucsd.edu

1 Materials Science Engineering Program, University of California San Diego, La Jolla, San Diego, CA 92093, USA

2 Division of Marine Science, University of Southern Mississippi, Stennis Space Center, MS 39529, USA

3 Seabird Scientific, 620 Applegate Street, Philomath, OR 97370, USA

4 School of Polymer Science and Engineering, The University of Southern Mississippi, Hattiesburg, MS 39406, USA

5 Department of Electrical and Computer Engineering, University of California San Diego, La Jolla, San Diego, CA 92093, USA

Published online: 17 May 2022

[22–29] of electronic materials so that electrochemical units can be easily incorporated into different layers within the microfluidic platform.

The prototype nitrate sensor in this report was integrated with two desalination units that lowered chloride concentrations resulting in improved sensor performance. The entire system was compact, with an area smaller than 5×4 cm^2 and fitted with an inexpensive (< USD \$15) mini-water pump that facilitated sample flow for monitoring changes in nitrate concentration at the sampling site. Our stacking approach extended the desalination path without increasing the device footprint, and the channel design also accounted for the voltage coupling between the desalination units and sensor to minimize voltage cross-talk. With the integration of a chloride removal process, the ISM sensor was shown to be sensitive enough to detect sub-millimolar levels of nitrate in seawater, of relevance to the standards set by the Environmental Protection Agency (EPA) [10]. This demonstration showed a promising point-of-use platform for nitrate detection in challenging samples with high concentration of dissolved salts. Moreover, the design is applicable to other types of anion sensors susceptible to interference by chloride.

Materials and methods

The microfluidic device consisted of two tandem desalination units and a downstream ISM nitrate sensor, as shown in Fig. 1a. The sample inlet was split into two separate streams, with one connected to a wide drain channel for displacing inline air bubbles and regulating flow rate, while the other channel entered the desalination process. Upon passing through the electrochemical redox units, the sample streams were separated into concentrated and desalinated seawater channels, indicated by dark and light blue colors, respectively. Subsequently, the desalinated channel fed into the potentiometric ISM sensor for measuring changes in nitrate concentration in the flowing sample. As such, the sample treatment and detection were implemented in one integrated, credit-card size compact platform.

The detailed design for each layer of the microfluidic device is shown in Fig. 1b and Supplemental Figure S1. The two tandem desalination electrochemical cells were patterned from layers 2 to 9, with Nafion ion-exchange membranes serving as separators embedded between layers 3 and 4, as well as between layers 7 and 8. The desalination units were stacked on top of each other, to minimize the device area footprint, while each unit increased the stack thickness by less than 0.5 mm. The serpentine channel in layer 10 increased the distance between the desalination unit and the sensor to mitigate parasitic voltage coupling. The sensor with an ISM of nitrate ion-exchange matrix [30] was placed on top of layer 11 to complete the fabrication.

We used low-cost patterning and assembly techniques, including digital cutting, stencil printing, and heat lamination, as summarized in Fig. 2a. Each layer was patterned from a 130-µm thick PET film, and areas were removed by a digital blade-cutter (Silhouette Cameo) to define the flow channels, electrode via holes, and alignment holes. Ag/AgCl ink (Ercon part# E2414) was printed through a stencil to

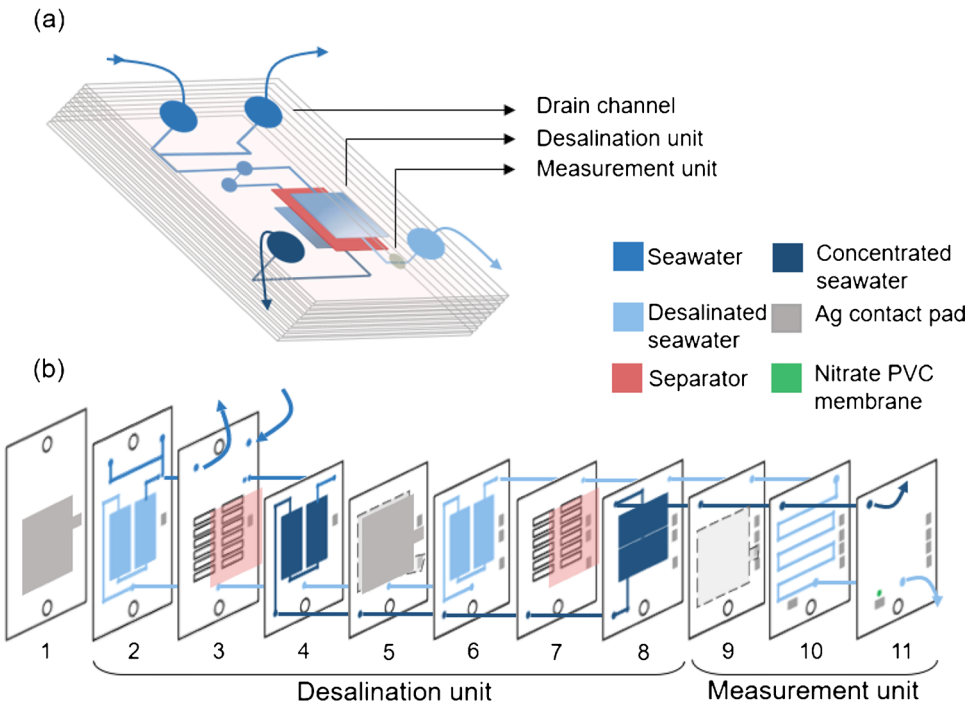

Fig. 1 (**a**) Schematics of the microfluidic platform with electrochemical desalination units preceding the nitrate sensor. (**b**) Exploded view of patterned layers to form flow channels embedded with electrochemical electrodes

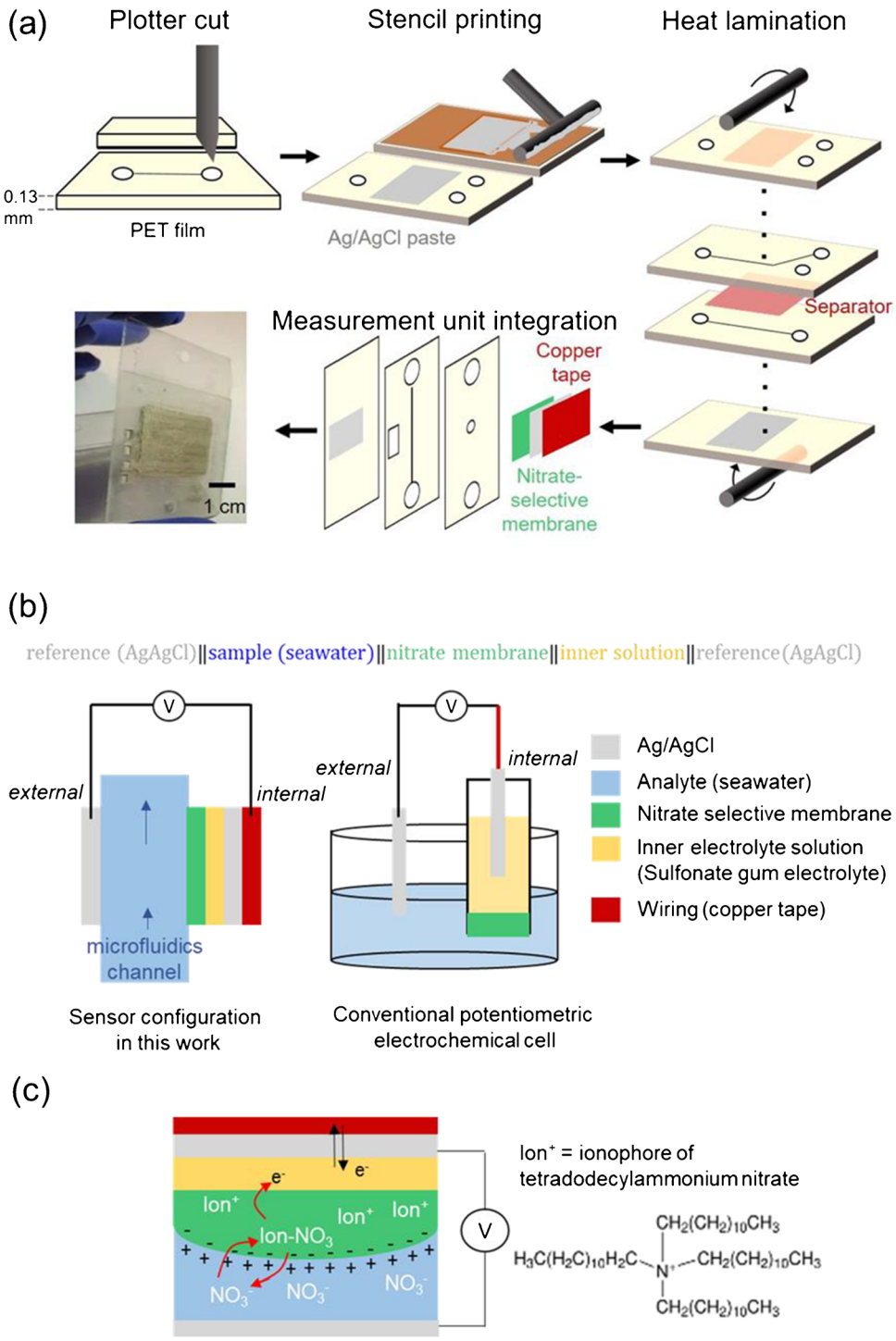

Fig. 2 (**a**) Schematics of fabrication methods for the microfluidic device. (**b**) Nitrate sensor structure (left), with an analogous design to conventional potentiometric electrochemical cell (right). (**c**) Illustration of the ion and charge exchange processes across the nitrate-selective membrane on the sensor

define the working electrode and counter/reference electrode with dimensions of 2.5 × 3 cm^2 on layers 1, 5, and 9 for the desalination units. Another electrode with dimensions of 0.2 × 0.1 cm^2 was printed on layer 10 as the external reference of the sensor in the sample channel. The Ag/AgCl patterns were dried at 85 °C for 30 min. In the assembly process, Nafion separators (part# 221) with thickness of 25.4 µm and areas of 4 × 4 cm^2 were inserted, and the entire stack of films were pressed between glass slides at 150 °C until the PET films looked transparent. The heat laminated the layers together by melting the adhesives on the PET films. The PET films came with the adhesive pre-attached for lamination.

Subsequently, the nitrate sensor electrode was attached on the top layer, followed by silicone encapsulation. The nitrate sensor was based on the configuration of a potentiometric electrochemical cell, as shown in Fig. 2b, with an external

electrode in contact with the sample solution and an internal electrode separated by an ion-selective membrane from the sample. We placed the sensor after the lamination step to avoid sensor degradation by high temperature, and this sequence also allowed facile exchange of sensors without the need to reassemble the microfluidic structure. Below are more specific descriptions of the sensor fabrication process and characterization equipment used for this work.

Preparation of the nitrate sensor electrode The nitrate-selective membrane was a modified version of a cocktail formulation [30] with the host matrix polyvinylchloride (PVC). The cocktail was prepared by mixing 1 ml of tetrahydrofuran, 64 mg of 2-nitrophenyl octyl ether, 32 mg of PVC, and 4 mg of tetradodecylammonium nitrate (TDAN). The selectivity coefficients of TDAN to different ions are listed in Table S1 [30]. The chemicals were purchased from Sigma-Aldrich and used as received. The solution was drop-cast onto a glass slide and allowed to dry over a day to form stand-alone films. Meanwhile, a piece of copper tape that would serve as the current collector was cleaned by acetone to remove the surface adhesive, and then Ag/AgCl ink was printed on the clean surface and annealed at 120 °C for 30 min to serve as the internal reference electrode of the sensor. To enable adhesion between the electrode and the nitrate-selective membrane, we used a gum electrolyte. The gum electrolyte was a solid-state film prepared by dissolving 1 g xanthan gum powder in 10 ml of 1-M sodium sulfate aqueous solution. The gum electrolyte served as an interface for charge exchange between the nitrate-selective membrane and the internal reference electrode. A thin paste of gum electrolyte ~ 100 µm was spread onto the Ag/AgCl electrode, followed by placement of the PVC nitrate-selective membrane. This sensor stack was put on the flow channel with the membrane in contact with the sample. The ion-exchange process at the membrane surfaces would lead to a potential difference if nitrate concentrations are not equal across the two sides of the ion-selective membrane. Thus, the analyte concentration was inferred by measuring the potential difference across the nitrate-selective membrane (Fig. 2b). The nitrate sensor was calibrated with a NIST-certified nitrate standard solution (40.0 mg/L NO_3-N in de-ionized water as received from Sigma-Aldrich) in Figure S2.

Pump system connection The mini water pump designed for aquariums and fountains was purchased from Ledgle and was run at 5 V during the experiment. The flow rate was tuned to be ~ 3.5 µl/s into the desalination cells. Samples in this work were artificial seawater prepared using Instant Ocean sea salt to reach a salinity of 31 g/kg, and the concentration of nitrate in the samples was adjusted by adding sodium nitrate into the water tank. The samples were pumped through a Teflon tube joint into the microfluidics device. The Teflon tube joint was held in place by magnetic force between magnetic gaskets (TJ250B, Amazing Magnets) and a magnetic plate sandwiching the microfluidic device, as shown in Figure S1.

Apparent salinity evaluation A salinity refractometer from Aichose was used to measure the sample after it passed through the desalination units. A multi-parameter water quality meter (Hanna model #HI98194) was used to calibrate the refractometer readings, as shown in Figure S3.

Electrochemical characterization Electrical control and readout were carried out with either a benchtop potentiostat (BioLogic SP-200) or a potable potentiostat (Metrohm µ300).

Results and discussion

Our desalination unit consisted of identical pairs of Ag/AgCl electrodes with a Nafion ion-exchange membrane in between. The Nafion membrane allowed sodium cations to pass through to maintain charge balance between the two coupled compartments with opposite salinity conditions. The Nafion membranes were activated through soaking under seawater over 10 min before use, in order to reach a steady-state condition (Figure S4). As shown in Fig. 3a, on the electrode at a positive potential, silver reacted with chloride ions selectively and formed silver chloride precipitates, resulting in chloride removal and reduction of water salinity in this compartment. In the complementary compartment with the electrode at a negative potential, chloride ions were released by silver chloride reduction, leading to an increased salinity in water on this side. Thus, the electrochemical process adjusted the chloride concentration and the associated salinity of the input seawater. The channel with increased Cl^- was directed to a discharge outlet, and the flow path of the de-chlorinated water was connected to the downstream sensor.

Figure 3b shows cyclic voltammetry (CV) of the Ag/AgCl electrode pair in artificial seawater of salinity 31 g/kg. The peak current and redox potentials were symmetric upon cyclic voltage sweeps, indicating that the electrochemical reactions were reversible. The wide peak-to-peak separation (1 ~ 2 V depending on the scan rate) was due to the sample solution resistance and manifested as an ohmic drop across the electrode pair. The potential for initiating desalination was around 0.5 V between the Ag/AgCl electrodes, and current magnitudes increased with a higher voltage scan rate. The peak current ($\log I$) versus scan rate ($\log V_s$) followed a power law relation $\log(I) = \log(a) + \log(V_s)$, as presented in Supplemental Figure S5, with fitted values of $a = 0.048$ and $b = 0.45$. The b value showed that the current

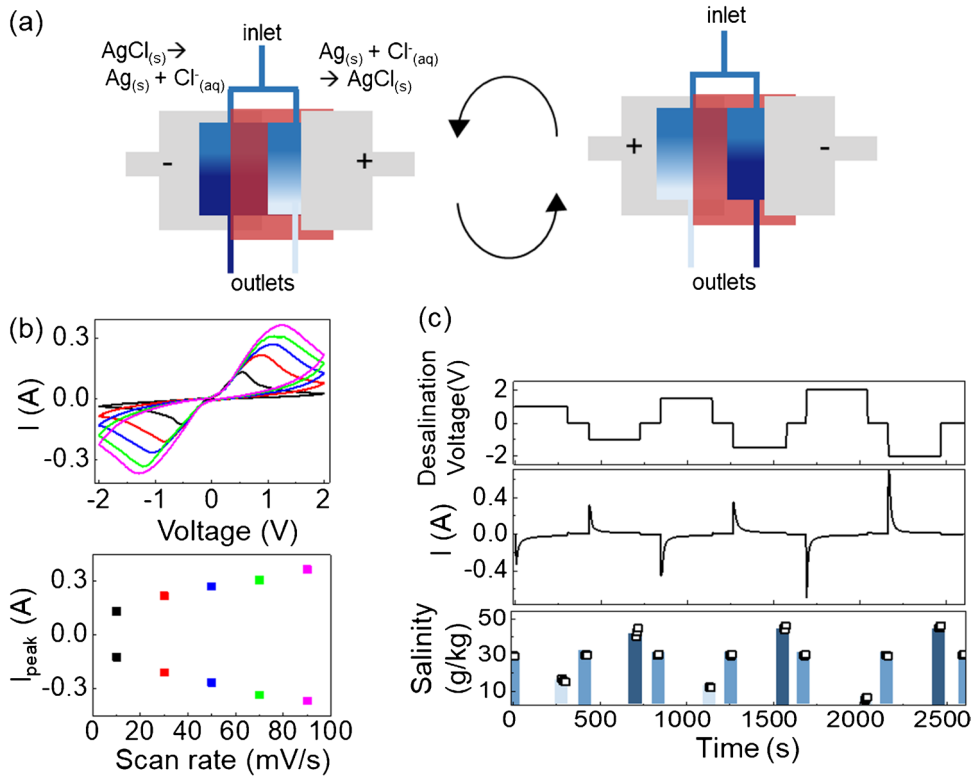

Fig. 3 (**a**) Schematics of the electrochemical desalination cell with Ag/AgCl ink. The blue areas indicate flow channels, and the red square is the Nafion separator. The components overlapped each other, as shown in Fig. 1, but here they were spread out for viewing clarity. (**b**) Top: cyclic voltammetry at scan rates from 10–90 mV/s, in increments of 20 mV/s. Bottom: peak current obtain from the above data versus scan rates. (**c**) Applied voltage on the desalination cell electrodes (top), corresponding measured current (middle), and measured salinity at the channel outlet (bottom) as a function of time. The data points of salinity were measured at the end of a period under a fixed voltage. The colors of the bars are guides to the eye, in which light blue indicates the sample is desalinated, medium blue is untreated (cell at 0 V), and dark blue is at a higher salinity level than the input sample due to regeneration of the electrode

was proportional to the square root of scan rates ($I \sim V_s^{0.5}$), indicating the desalination process here was a diffusion-controlled reaction according to the Randles–Sevcik Eq. [31, 32].

Figure 3c displays the change in water salinity level as a function of the applied voltage. While the sample was constantly flowing at ~ 3.5 µl/s into the desalination cells, a constant voltage was applied on the electrode for 5 min and then turned off to 0 V for 2 min to replenish the compartment with untreated seawater. After the 2-min off period, the electrodes were biased for another 5 min at the same voltage magnitude but with an opposite polarity to the previous on-period, to reverse Ag/AgCl reactions and refresh electrode surfaces for the next cycle of desalination. At the end of each biasing condition, the apparent salinity was measured in-line with a calibrated refractometer. The apparent salinity decreased from the initial values of 31 to 15, 12, and 6, at 1 V, 1.5 V, and 2 V, respectively, for the compartment with the electrode at positive biases. When negative potentials were applied to refresh the Ag/AgCl electrode, the apparent salinity increased to 43, 46, and 45, at − 1 V, − 1.5 V, and − 2 V, respectively. A smaller salinity change is observed during regeneration (from the unprocessed sample with 31 g/kg to 45 g/kg, a change of 14 g/kg) than during desalination (from 31 g/kg to 6 g/kg, a change of 25 g/kg). We think that the initial ratio of Ag/AgCl in our electrodes is probably not equal in composition and might contain less AgCl. Thus less AgCl is reduced during regeneration, leading to less Cl^- ion being released and a smaller change in salinity. Furthermore, we calculated the desalination efficiency, defined as the ratio of salt *removed* to the original amount, from the measured chloride concentration changes [13, 33, 34] after passing through two stages. Converting apparent salinity to NaCl molar concentration, 31 g/kg = 0.5 M and 6 g/kg = 0.1 M, the amount of NaCl removed from the seawater sample at 2 V was 0.4 M. Thus, the desalination efficiency reached 0.4 M /0.5 M = 80% in our tandem device.

During the integration of desalination units and the nitrate sensor, the channel distance between the two should be carefully planned to mitigate parasitic voltage coupling, particularly because seawater acted as a conductive electrolyte between the electrodes in contact with it. Previously, voltage

cross-talk was reduced by physical isolation of channels, using mechanical valves or introducing air bubbles [13–15]. However, in order to reduce the complexities in fabrication and control electronics, here, we simply extended the distance between desalination units and the sensor. A long serpentine path increases the electrical resistance and thus leads to a sufficient voltage drop to make the cross-talk negligible.

Figure 4a shows the different locations at which the cross-talk voltage was measured when a pulse of 0.5 V was applied on the desalination electrodes. In the equivalent circuit model, the resistance due to electrolyte path-lengths is expressed as a variable resistor $R_s(D)$, with D being the distance parameter. The fixed resistors encompassed the resistance of the electrodes and other components such as separator and nitrate-selective membranes. Figure 4b presents the cross-talk voltage (ΔV) at the sensor electrodes as the desalination units were turned on and off. The extent of cross-talk was calculated as a percentage, defined as $\% = \Delta V/V_{desal}$, where V_{desal} was the applied desalination voltage = 0.5 V in this measurement. The cross-talk % decreased to less than 1% and became negligible when the channel path-length was longer than 20 cm. Hence, we used a serpentine length of 27 cm as the connection path between the desalination units and the sensor.

Upon integration of the potentiometric nitrate sensor with the desalination units, we tested this microfluidic platform in Fig. 5a for its sensitivity and detection limit for nitrate analytes in seawater. When the desalination units were not used, changes in nitrate concentration in the untreated seawater were not distinguishable from the background drift of the sensor open-circuit voltage, as shown in Fig. 5b. A comparison with prior works shows this same issue, as summarized in Table S2. When the desalination units were turned on to reduce chloride interference, the sensor response to changes in nitrate concentration is much more obvious in Fig. 5c. With 2 V at the desalination units, the sample flowing into the nitrate sensor was de-chlorinated, and the sensor voltage was measured to change from 19.4 to 1.9 mV as the nitrate concentration was varied from 10^{-4} to 10^{-2} M. (We also include Supplemental Figure S7 that demonstrated a similar response when the input nitrate concentration is changed across two orders of magnitudes over a shorter interval of 3 min, more quickly than in Fig. 5). After the analyte detection period, the applied voltage to desalination units was switched to − 2 V for reducing AgCl back to Ag for the next cycle of desalination and detection. The sensor during this regeneration period was not sensitive to nitrate concentration, with the voltage changing by < 8 mV, in comparison to > 18 mV response for 10^{-3} M nitrate when there was minimal chloride interference during desalination.

The voltage dependence of the nitrate potentiometric sensor is expressed as

$$V = \frac{kT}{ze} \ln Q_r - \frac{\int Idt}{C_{AgCl}} + \text{constant}, \quad (1)$$

where Q_r is the activity coefficient dependent on the analyte concentration; the parameter T is the temperature; k is the Boltzmann constant; e is the electron charge; and z is the number of electrons transferred in the redox reaction. C_{AgCl} is the capacitance of Ag/AgCl electrodes at the desalination units. The term $\int Idt$ is the transferred charge during the desalination process and $\int Idt$ is dependent on the redox current I integrated over time. We neglected the cross-talk voltage, as it has been minimized and would be a constant voltage offset even if it was present. The second term in Eq. (1) accounts for the small gradual voltage shift during the detection period, because of the on-going desalination

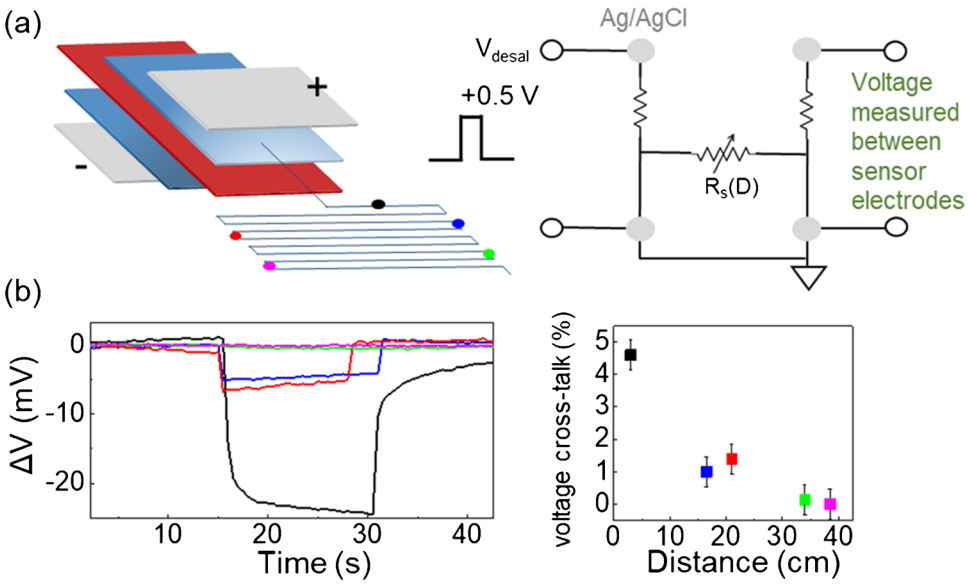

Fig. 4 (**a**) Schematic of the voltage coupling measurements at increasing path lengths away from the desalination unit as indicated by the different color points. An equivalent circuit model representing the path between desalination electrodes and sensor electrodes is shown on the right. (**b**) Measured open-circuit voltage at the sensor electrodes when desalination electrodes were at 0.5 V. The data point colors correspond to the locations in part a

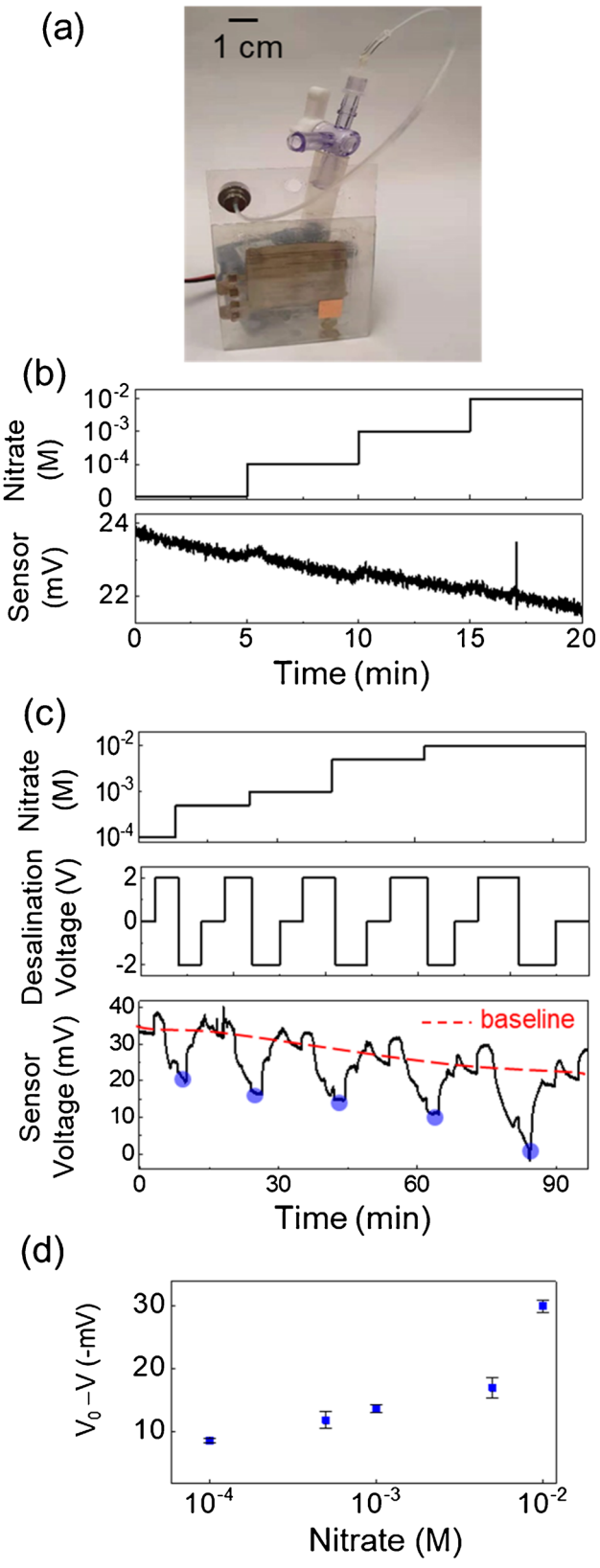

Fig. 5 (**a**) Photograph of the point-of-use microfluidic system for nitrate detection. (**b**) Sensor response as nitrate concentration was varied in the sample without de-chlorination treatment. The starting concentration is 10^{-4} M nitrate. (**c**) Sensor response to nitrate in the sample with de-chlorination treatment. There is a ~ 2-min offset between voltage switching and sensor response due to the flow distance. The dashed baseline represents the sensor response when the desalination units were off while the nitrate concentration was varied. (**d**) Difference in the sensor open-circuit voltage V and the baseline V_0 versus nitrate concentrations, taken at the time points as indicated by the blue dots in part c. The error bars were obtained from running the sensor for three trials

process that concurrently changed the chloride concentration in the sample and also changed the silver electrode capacitance during the electrochemical process.

The device settling time after turning on the desalination units was around 8 min, and this time was dependent on the flow rate and the time to establish equilibrium between the two sides of the nitrate-selective membrane. The stability of this microfluidics device is mainly limited by the desalination units, while the sensor electrodes are not significantly affected by residual chloride in the sample. To extend the usable time of the desalination units, we leveraged reversible redox reactions to refresh the electrodes. Each pair of desalination Ag/AgCl electrodes was separated by the Nafion exchange membrane. The voltage polarity on each electrode is switched in every cycle. In one electrode Ag is oxidized with chloride ions to form AgCl precipitates, while its complementary electrode is reduced and the AgCl precipitated from the prior cycle is recovered back to Ag for the next cycle of oxidation. By incorporating this refresh step, the usable time of the desalination electrode pair is greatly improved from a few seconds to more than 1 h. The microfluidic platform was operated continuously for 4000 s in Figure S8, and the desalination efficiency dropped from 80 to 50% due to the deposition of AgCl on the Nafion separator membrane [13, 35] that blocked some of the sodium ion transport pathways. The increased desalination cell resistance was suggested by the redox potential shift, as shown in the cyclic voltammetry in Supplemental Figure S9c.

The blue points in Fig. 5c mark the voltage measured at the end of each period of desalination and detection, and are presented in Fig. 5d to extract the sensitivity and limit of detection for nitrates. For our platform, the sensitivity was 11.3 mV/dec for nitrate concentration between 10^{-3} and 10^{-2} M, and the detection limit was 0.5 mM (with an average sensitivity of 9.8 mV/dec in Figure S10 comparing three fabrication batches). These sensitivity levels were similar to the results of an individual nitrate sensor operating with 0.1 M chloride in the background (12.9 mV/dec in Figure S6 and 99% response recovery in Figure S11). Since the U.S. EPA standards [10] standard for nitrate concentration in drinking water is 44 ppm (0.7 mM), the detection limit of our

point-of-use platform was sufficient to identify unsafe nitrate concentration for human health.

Conclusions

A low-cost, portable microfluidic platform has been developed to detect nitrate at millimolar levels in seawater. The cut-and-laminate fabrication process enables rapid and easy integration of desalination units and ISM potentiometric sensors. The desalination efficiency was up to 80% using two tandem electrochemical cells. The channel length between the desalination and nitrate sensor was optimized to minimize voltage cross-talk. The point-of-use microfluidic platform showed the feasibility of inline analyte monitoring for challenging seawater samples with a ~ 31 g/kg salinity at the input.

The sensitivity and detection limit of this platform can be improved by incorporating more desalination units in tandem to raise the desalination efficiency. The problem with precipitation on the desalination separator may be improved by using a higher flow rate and increasing the distance between the electrodes and the separator. In addition to nitrate sensing, the platform described herein can potentially be extended to other analytes affected by high background chloride concentration, such as phosphate. Overall, our work demonstrates an approach to reduction in the size, weight, and cost of chemical sensor systems for saline waters.

Supplementary Information The online version contains supplementary material available at https://doi.org/10.1007/s00604-022-05314-5.

Acknowledgements This project was supported by Office of Naval Research award N00014-19-1-2687.

Declarations

Conflict of interest The authors declare no competing interests.

References

1. Jani J, Yang YY, Lusk MG, Toor GS (2020) Composition of nitrogen in urban residential stormwater runoff: concentrations, loads, and source characterization of nitrate and organic nitrogen. PLoS One 15(2):e0229715
2. Chen X, Zhou G, Mao S, Chen J (2018) Rapid detection of nutrients with electronic sensors: a review. Environ Sci Nano 5(4):837–862
3. Patey MD, Rijkenberg MJA, Statham PJ, Stinchcombe MC, Achterberg EP, Mowlem M (2008) Determination of nitrate and phosphate in seawater at nanomolar concentrations. Trends Anal Chem 27(2):169–182
4. Wu S, Yao L, Shiller A, Barnard AH, Azoulay JD (2021) Dual-gate organic electrochemical transistors for marine sensing. Adv Electron Mater 7:2100223
5. Alahi MEE, Mukhopadhyay SC (2018) Detection methods of nitrate in water: a review. Sens Actuators A 280:210–221
6. Minami T, Sasaki Y, Minamiki T, Wakida S, Kurita R, Niwa O, Tokito S (2016) Selective nitrate detection by an enzymatic sensor based on an extended-gate type organic field-effect transistor. Biosens Bioelectron 81:87–91
7. Morales JA, De Graterol LS, Mesa J (2000) Determination of chloride, sulfate and nitrate in groundwater samples by ion chromatography. J Chromatogr A 884(1–2):185–190
8. Jobgen WS, Jobgen SC, Li H, Meininger CJ, Wu G (2007) Analysis of nitrite and nitrate in biological samples using high-performance liquid chromatography. J Chromatogr B Anal Technol Biomed Life Sci 851(1–2):71–82
9. Bao C, Kim WS (2020) Perspective of printed solid-state ion sensors toward high sensitivity and selectivity. Adv Eng Mater 22(8):2000116
10. Sohail M, Adeloju SB (2008) Electroimmobilization of nitrate reductase and nicotinamide adenine dinucleotide into polypyrrole films for potentiometric detection of nitrate. Sens Actuators B Chem 133(1):333–339
11. Gallardo J, Alegert S, Del Valle M (2004) A flow-injection electronic tongue based on potentiometric sensors for the determination of nitrate in the presence of chloride. Sens Actuators B Chem 101(1–2):72–80
12. Roelofs SH, Van Den Berg A, Odijk M (2015) Microfluidic desalination techniques and their potential applications. Lab Chip 15(17):3428–3438
13. Cuartero M, Crespo GA, Bakker E (2015) Tandem electrochemical desalination-potentiometric nitrate sensing for seawater analysis. Anal Chem 87(16):8084–8089
14. Fighera M, van der Wal PD, Shea H (2017) Microfluidic platform for seawater desalination by coulometric removal of chloride ions through printed Ag electrodes. J Electrochem Soc 164(12):H836–H845
15. Nge PN, Rogers CI, Woolley AT (2013) Advances in microfluidic materials, functions, integration, and applications. Chem Rev 113:2550
16. Zarabadi MP, Paquet-Mercier F, Charette SJ, Greener J (2017) Hydrodynamic effects on biofilms at the biointerface using a microfluidic electrochemical cell: case study of Pseudomonas sp. Langmuir 33(8):2041–2049
17. Pavesi A, Piraino F, Fiore GB, Farino KM, Moretti M, Rasponi M (2011) How to embed three-dimensional flexible electrodes in microfluidic devices for cell culture applications. Lab Chip 11(9):1593–1595
18. Zeng S, Wen C, Zhang SL, Zhang Z (2020) A nanopore array of individual addressability enabled by integrating microfluidics and a multiplexer. IEEE Sens J 20(3):1558–1563
19. Jin JH, Kim JH, Lee SK, Choi SJ, Park CW, Min NK (2018) A Fully Integrated Paper-Microfluidic Electrochemical Device for Simultaneous Analysis of Physiologic Blood Ions. Sensors (Switzerland) 18(1):104
20. Kim J, Kim J, Shin Y, Song S, Lee J (2014) Rapid prototyping of multifunctional microfluidic cartridges for electrochemical biosensing platforms. Sens Actuators B Chem 202:60–66
21. Thompson BL, Ouyang Y, Duarte GRM, Carrilho E, Krauss ST, Landers JP (2015) Inexpensive, rapid prototyping of microfluidic devices using overhead transparencies and a laser print, cut and laminate fabrication method. Nat Protoc 10(6):875–886
22. Kwon KS, Rahman MK, Phung TH, Hoath SD, Jeong S, Kim JS (2020) Review of digital printing technologies for electronic materials. Flex Print Electron 5(4):043003
23. Zhai Y, Wang Z, Kwon KS, Cai S, Lipomi D, Ng TN (2020) Printing multi-material organic haptic actuators. Adv Mater 2002541.
24. Wang K, Huang L, Eedugurala N, Zhang S, Sabuj MA, Rai N, Gu X, Azoulay JD, Ng TN (2019) Wide potential window

supercapacitors using open-shell donor–acceptor conjugated polymers with stable N-doped states. Adv Energy Mater 1902806.
25. Yao L, Liu J, Eedugurala N, Mahalingavelar P, Adams DJ, Wang K, Mayer KS, Azoulay JD, Ng TN (2022) Ultrafast high-energy micro-supercapacitors based on open-shell polymer-graphene composites. Cell Rep Phys Sci 100792.
26. Atreya M, Dikshit K, Marinick G, Nielson J, Bruns C, Whiting G (2020) Poly (Lactic acid)-based ink for biodegradable printed electronics with conductivity enhanced through solvent aging. ACS Appl Mater Interfaces 12:23494
27. Bonnassieux Y, Brabec CJ, Cao Y, Carmichael TB, Chabinyc ML, Cheng K, Cho G, Chung A, Cobb CL, Distler A, Egelhaaf H-J, Grau G, Guo X, Haghiashtiani G, Huang T-C, Hussain MM, Iniguez B, Lee T, Li L, Ma Y, Ma D, McAlpine MC, Ng TN, Osterbacka R, Patel S, Peng J, Peng H, Rivnay J, Shao L, Steingart D, Street RA, Subramanian V, Torsi L, Wu Y (2021) The 2021 flexible and printed electronics roadmap. Flex Print Electron 6:023001
28. Huang Q, Al-Milaji KN, Zhao H (2018) Inkjet printing of silver nanowires for stretchable heaters. ACS Appl Nano Mater 1:4528
29. Amit Moran, Mishra Rupesh K, Hoang Quyen, Galan Aida Martin, Wang Joseph, Ng Tse Nga (2019) Point-of-use robotic sensors for simultaneous pressure detection and chemical analysis. Materials Horizons 6(3):604–611. https://doi.org/10.1039/C8MH01412D
30. Campanella L, Colapicchioni C, Crescentini G, Sammartino MP, Su Y, Tomassetti M (1995) Sensitive membrane ISFETs for nitrate analysis in waters. Sens Actuators B Chem 27(1–3):329–335
31. Kim T, Choi W, Shin HC, Choi JY, Kim JM, Park MS, Yoon WS (2020) Applications of voltammetry in lithium ion battery research. J Electrochem Sci Technol 11(1):14–25
32. Wang K, Yao L, Jahon M, Liu J, Gonzalez M, Liu P, Leung V, Zhang X, Ng TN (2020) Ion-exchange separators suppressing self-discharge in polymeric supercapacitors. ACS Energy Lett 5:3276–3284
33. Cuartero M, Crespo G, Cherubini T, Pankratova N, Confalonieri F, Massa F, Tercier-Waeber M-L, Abdou M, Schäfer J, Bakker E (2018) In situ detection of macronutrients and chloride in seawater by submersible electrochemical sensors. Anal Chem 90(7):4702–4710
34. Pankratova N, Cuartero M, Cherubini T, Crespo GA, Bakker E (2017) In-line acidification for potentiometric sensing of nitrite in natural waters. Anal Chem 89(1):571–575
35. Cuartero M, Crespo GA, Ghahraman Afshar M, Bakker E (2014) Exhaustive thin-layer cyclic voltammetry for absolute multianalyte halide detection. Anal Chem 86(22):11387–11395